

## Total Cross Sections for Multiple Electron Stripping in Atomic Collisions at Energies to 100 keV\*

P. R. JONES,† F. P. ZIEMBA, H. A. MOSES, AND E. EVERHART  
*Physics Department, University of Connecticut, Storrs, Connecticut*

(Received August 8, 1958)

Total cross sections have been measured for electron capture and stripping of He<sup>+</sup>, Ne<sup>+</sup>, and A<sup>+</sup> ions in single collisions of He<sup>+</sup> on He, Ne, and A; Ne<sup>+</sup> on Ne and A; and A<sup>+</sup> on A. Where He<sup>+</sup> ions are incident, the cross sections are given for electron capture,  $\sigma_{10}$ ; for electron loss,  $\sigma_{12}$ ; and for "elastic" scattering in excess of one degree,  $\sigma_{11} > 1^\circ$ . Where Ne<sup>+</sup> and A<sup>+</sup> are incident, the cross sections for multiple stripping  $\sigma_{13}, \dots, \sigma_{17}$  are given also. The measurements were made at 25, 50, and 100 keV and at additional energies in two cases where a maximum in the electron capture cross section was observed. Each total cross section was compiled by adding the contributions from the various angular regions into which the incident particle may be scattered. The contribution from the particles scattered between 0° and 1° was measured directly, while that for regions in excess of 1° was obtained by integrating the measured differential cross sections. In the region between 1° and 4° the differential cross section for each process was measured with high resolution and these data are presented here separately. These differential measurements supplement data previously published for angles in excess of 4°. Tables are presented showing the contribution of each of the angular regions to the various total cross sections. Large-angle scattering is found to make a significant contribution to the total cross sections for the production of the more highly ionized particles.

### 1. INTRODUCTION

TOTAL cross sections for the multiple stripping of an ion in single collisions with an atom may evidently be obtained by integrating the measured differential cross sections over all angles of scattering. Previous differential measurements of single collisions of helium, neon, and argon ions and atoms at energies of 25 to 100 keV have been reported by this laboratory in two papers,<sup>1,2</sup> hereinafter called I and II, respectively. Similar studies have been reported by Fedorenko<sup>3</sup> and by Kaminker and Fedorenko.<sup>4</sup> These investigations have shown that for the higher charge states important contributions to total cross sections arise from large-angle scattering.

Measured values of the total cross sections are given here for processes in which a singly ionized atom strikes a neutral target atom and is 0, 1, 2, to 7 times ionized after the collision. These are called, respectively, the cross sections for electron capture (sometimes called charge exchange), "elastic" scattering, and various degrees of multiple stripping. The collisions studied include He<sup>+</sup> incident on He, Ne, and A; Ne<sup>+</sup> on Ne and A; and A<sup>+</sup> on A at energies of 25, 50, and 100 keV. The electron capture cross sections are compared with those of a number of other investigators. In the case of "elastic" scattering the cross section for

scattering in excess of 1 degree was measured. These collisions are "elastic" in the sense that there is no change of charge, but there may be an excited state created and photons emitted which are not detected in these measurements. For some of the higher charge states Kaminker and Fedorenko<sup>4</sup> show data on the cross sections for stripping which may be compared with our results.

The procedure is to determine the contribution to the total cross section arising from each of the several regions into which the incident particle may be scattered. The differential cross section measurements for the 1 to 4 degree region are reported here in Sec. 2. The 0 to 1 degree measurements are discussed in Sec. 3 to follow. The data for the region in excess of 4 degrees are obtained from paper II. The total cross sections obtained in this way are presented and discussed here in Sec. 4.

### 2. MEASUREMENTS FROM 1 TO 4 DEGREES

#### a. Apparatus

The scattering apparatus shown in Fig. 1(a) is essentially that described in II. This apparatus measures the scattered incident particle current in each charge state resulting from single collisions with target gas atoms as a function of scattering angle  $\theta$ . In II it was used to study the range of angles above 4 degrees, extending up to 40 degrees in some cases. Here it has been adapted to make measurements in the 1 to 4 degree range. This entailed making the holes smaller to provide the necessary resolution. The extreme angular width of acceptance is now  $\pm 0.2$  degree although about three quarters of the scattered particles come from a range of  $\pm 0.1$  degree about the chosen angle  $\theta$ .

\* This work was sponsored by the Office of Ordnance Research U. S. Army, through the Ordnance Materials Research Office at Watertown and the Springfield Ordnance District.

† Now at the University of Massachusetts, Amherst, Massachusetts.

<sup>1</sup> Carbone, Fuls, and Everhart, *Phys. Rev.* **102**, 1524 (1956). Here referred to as I.

<sup>2</sup> Fuls, Jones, Ziemba, and Everhart, *Phys. Rev.* **107**, 704 (1957). Here referred to as II.

<sup>3</sup> N. V. Fedorenko, *Zhur. Tekh. Fiz.* **24**, 784 (1954).

<sup>4</sup> D. M. Kaminker and N. V. Fedorenko, *Zhur. Tekh. Fiz.* **25**, 2239 (1955).

**b. Theory and Procedure**

The particle differential cross section is the area of the scattering center for scattering of particles, irrespective of their charge after scattering, into a unit solid angle at the angle in question. This is found from the data through the expression

$$\sigma(\theta) = I/NmL\Delta\Omega, \quad (1)$$

where  $I$  is the number of scattered particles per second of all charge states detected at the angle  $\theta$ ,  $N$  is the number of incident particles per second,  $m$  is the number of target particles per unit volume,  $L$  is the length of the target volume in the direction of the incident ion beam, and  $\Delta\Omega$  is the effective solid angle over which the average value of the particle differential cross section  $\sigma(\theta)$  is determined.

The value of  $\Delta\Omega$  is determined by the scattering geometry, which is shown in more detail in Fig. 2 of II, and is the average solid angle of scattering over the target volume. The integration over the target volume yields

$$\Delta\Omega = \pi S^2 h / [4y_2(y_1 S + y_2 h)], \quad (2)$$

where  $S$  is the diameter of hole  $d$  in Fig. 1(a),  $h$  is the height of the rectangular hole  $c$ ,  $y_1$ , and  $y_2$  are the distances from the point  $b$  of holes  $c$  and  $d$ , respectively. Here  $S = 0.15$  mm,  $h = 0.08$  mm,  $y_1 = 24.2$  mm, and  $y_2 = 57.8$  mm.

The length  $L$  is given by

$$L = \frac{1}{2} [\csc(\theta - |\Delta\theta|) + \csc(\theta + |\Delta\theta|)] (y_2 h + y_1 S) / (y_2 - y_1), \quad (3)$$

where  $\Delta\theta = \pm 0.2$  degree is the extreme angular width of acceptance determined by the holes  $c$  and  $d$ . For large values of the scattering angle  $\theta$ , this expression is well approximated by Eq. (2) of II. Substitution of Eqs. (2) and (3) into Eq. (1) gives an expression for  $\sigma(\theta)$  in which everything can be measured.

At each scattering angle  $\theta$  in the 1 to 4 degree range the scattered particle current  $I_n$  in each charge state  $n$  was measured, and from these data the fraction  $P_n$  of the scattered particles in each charge state determined. Each data set included some very small scattering angles  $\theta$  for which the data was obtained in two ways—with the detecting apparatus in Fig. 1(a) rotated an angle  $\theta$  first above, and then below, the incident ion beam direction. An average of these two values was recorded. The scattered currents at small angles are very rapidly changing functions of angle and this procedure corrects for errors, of the order of 0.1 degree, in alignment between the direction of the ion beam and the zero index on the angle scale.

Immediately after each data set was taken, the target gas supply to the collision chamber was shut off and the experiment repeated to determine the scattered currents due to residual gas atoms or any other extraneous source. The pressure in the collision chamber was

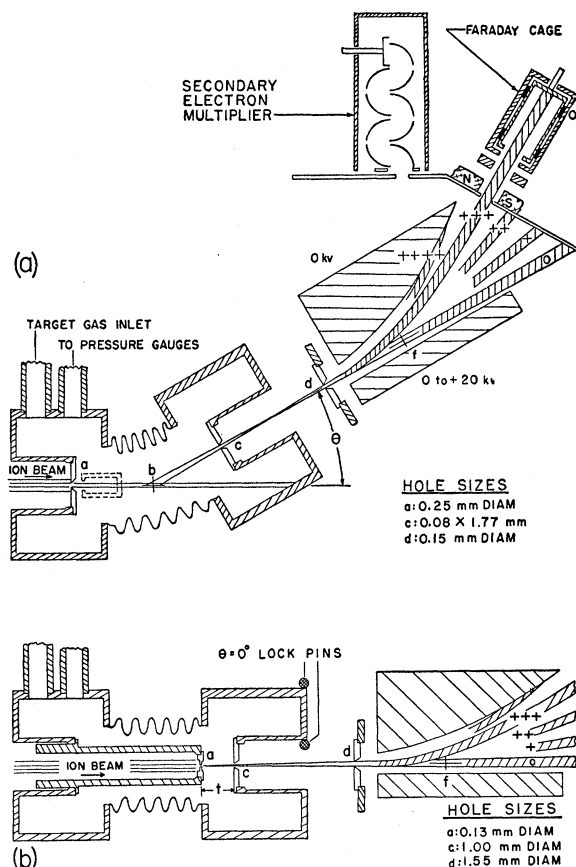


FIG. 1. The scattering apparatus used (a) in the 1 to 4 degree measurements and (b) adapted to the 0 to 1 degree measurements.

then about  $5 \times 10^{-6}$  mm of Hg, this being the pressure in the accelerator to which this chamber is connected. This compares with a pressure of about  $10^{-3}$  mm of Hg in the chamber with the target gas supply turned on. The scattered currents were found to be about 5% of the value they had when the target gas was present, except for certain cases of  $\text{He}^+$  on He when they reached 15%. In every case these were subtracted from the corresponding currents measured with the target gas present.

**c. Data and Discussion**

The charge analysis of the scattered particles and the particle differential scattering cross sections are shown in Figs. 2 through 7 for collisions of  $\text{He}^+$  on He, Ne, and A;  $\text{Ne}^+$  on Ne and A; and  $\text{A}^+$  on A at energies of 25, 50, and 100 kev. The fraction  $P_n$  of scattered particles in each charge state, and the particle differential scattering cross section, are shown at each energy as a function of the scattering angle  $\theta$  in laboratory coordinates. Each data point represents the average of two or more determinations from experiments performed on different days. Empirical lines are drawn through the charge analysis data points.

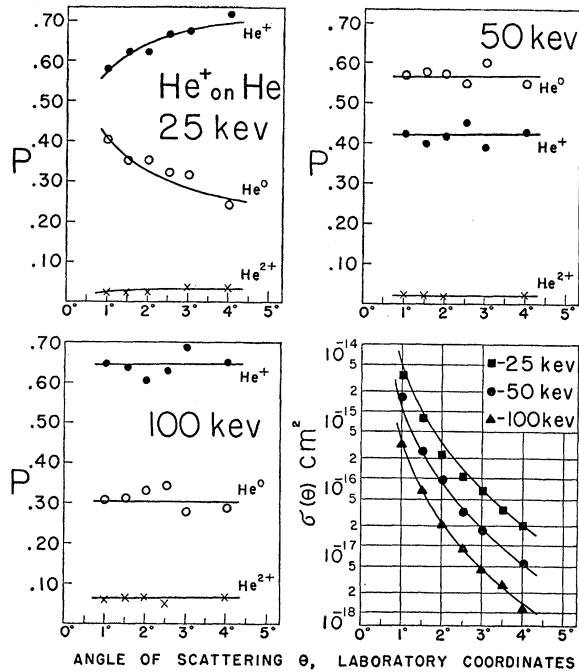


FIG. 2. The charge analysis and differential scattering cross sections for single collisions of  $\text{He}^+$  on He at 25, 50, and 100 keV. The fraction of scattered particles in each charge state is plotted vs scattering angle and empirical lines drawn through the data points. The differential cross section is plotted vs scattering angle, the solid lines being calculated using the Rutherford scattering formula. These data are an extension to small angles of the data in Figs. 4 and 10 of reference II.

When helium ions are the incident particles the fraction  $P_n$  is observed to be entirely independent of the scattering angle  $\theta$  at 100 keV, and nearly so at 50 keV. The variation of  $P_n$  with  $\theta$  is seen to be present only in the range of gentler collisions, encountered at low-energy and small angles of scattering, corresponding to large impact parameters for the collisions. A variation of  $P_n$  with the energy of the incident helium ion is also observed. When neon and argon ions are incident upon neutral neon and argon atoms,  $P_n$  is seen to vary considerably with  $\theta$  as well as with the incident ion energy. A theoretical treatment of the  $\text{A}^+$  on A collision has been given by Russek and Thomas.<sup>5</sup> Their calculations reproduce quite well the general behavior of  $P_n$  as a function of  $\theta$  observed here and in reference II.

The measured particle differential scattering cross section for collisions of  $\text{He}^+$  on He is compared in Fig. 2 with that calculated using the Rutherford scattering formula. In these collisions the effect of electron screening is negligible and the observed scattering should be given quite accurately as that calculated from a Coulomb potential. The excellent agreement of the data points with the Rutherford curves is taken as evidence that there was no excessive systematic error in the differential cross-section measurements.

<sup>5</sup> A. Russek and M. Tom Thomas, Phys. Rev. **109**, 2015 (1958).

### 3. MEASUREMENTS FROM 0 TO 1 DEGREE

#### a. Apparatus

Figure 1(b) shows the apparatus as adapted to the analysis of scattered particles which have been deflected by less than 1 degree from the incident ion beam. No differential cross section measurements were attempted below 1 degree and the design here is such that all particles scattered by less than 1 degree enter the detectors, separated only according to their charge. The circular hole  $d$  subtends a linear angle of 2 degrees from  $a$  and  $2\frac{1}{2}$  degrees from  $c$ , so that particles scattered into a 1-degree radius cone at  $a$  and a  $1\frac{1}{4}$ -degree cone at  $c$  reach the detectors. In this part of the experiment the incident ion beam entered the collision chamber with a collimation of  $\pm 0.1$  degree and traversed a thickness of 8.9 mm of target gas.

#### b. Theory and Procedure

The contributions to the total cross section  $\sigma_{1n}$  by the 0 to 1 degree region is given by

$$\sigma_{1n}^*(0^\circ \rightarrow 1^\circ) = I_n / Nmt, \quad (4)$$

where  $I_n$  is the particle current of  $n$ -times ionized atoms resulting from target gas collisions,  $N$  is the incident particle current of singly ionized atoms,  $m$  is the number of targets per unit volume, and  $t$  is the

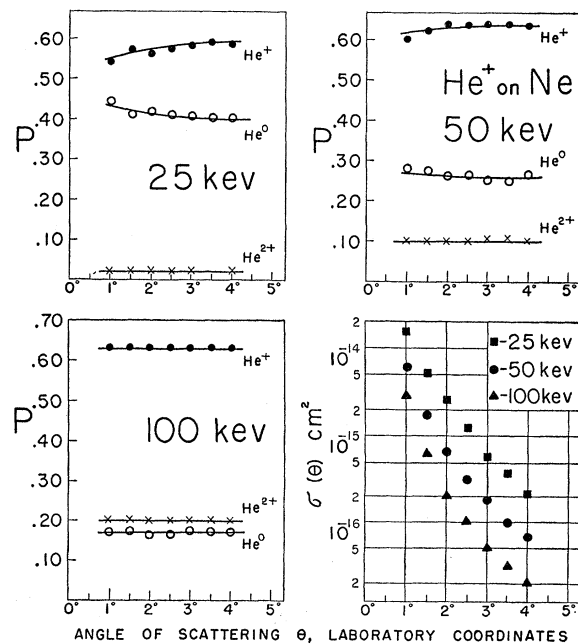


FIG. 3. The charge analysis and differential scattering cross sections for single collisions of  $\text{He}^+$  on Ne at 25, 50, and 100 keV. The fraction of scattered particles in each charge state is plotted vs scattering angle and empirical lines drawn through the data points. The differential cross section is plotted vs scattering angle. These data are an extension to small angles of the data in Figs. 5 and 11 of reference II.

thickness of the target in the direction of the ion beam. All quantities in this expression can be measured.

The apparatus was here locked as shown in Fig. 1(b) so as to prevent rotation about point *b*. The particle current in each charge state was determined at several target gas pressures as shown in Fig. 8. The linear plot shows that the particles reaching the detector had undergone only single interactions. In practice,  $\sigma_{1n}^*(0^\circ \rightarrow 1^\circ)$  was determined by the slope of the best straight line through the data points since this is proportional to the factor  $I_n/Nm$  in Eq. (4).

The residual current shown at "zero" pressure in Fig. 8 was the steady value reached after the target gas supply to the collision chamber had been shut off for several minutes. The principal source of this extraneous current is the interaction of the ion beam with impurity gases in the long path outside the collision chamber where the pressure is about  $5 \times 10^{-6}$  mm of Hg. This current makes no contribution when  $\sigma_{1n}^*(0^\circ \rightarrow 1^\circ)$  is determined from the slope of the straight line as described above.

It was found in the 0 to 1 degree measurements that target gas atoms outside of the collision chamber, as well as impurity gases, give rise to a significant fraction of the observed particle current in a given charge state. These atoms stream out through holes *a* and *c* which are necessarily open. Although the target gas pressure outside the chamber was only about 0.01 of that inside the chamber, the much longer path length of the beam

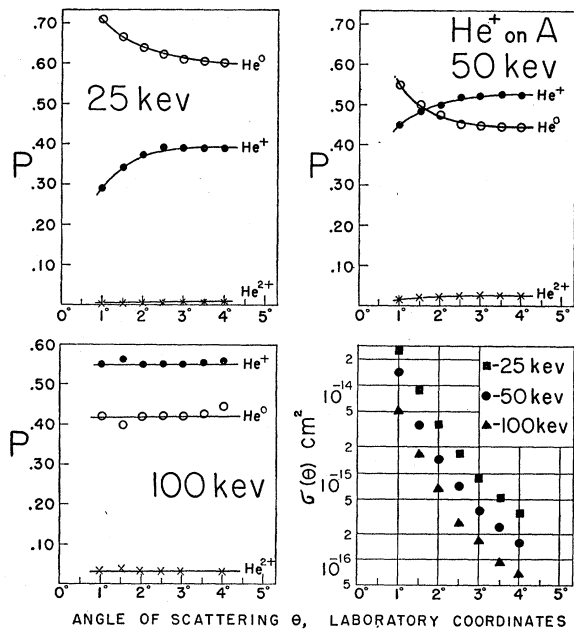


FIG. 4. The charge analysis and differential scattering cross sections for single collisions of  $\text{He}^+$  on A at 25, 50, and 100 keV. The fraction of scattered particles in each charge state is plotted *vs* scattering angle and empirical lines drawn through the data points. The differential cross section is plotted *vs* scattering angle. These data are an extension to small angles of the data in Figs. 6 and 12 of reference II.

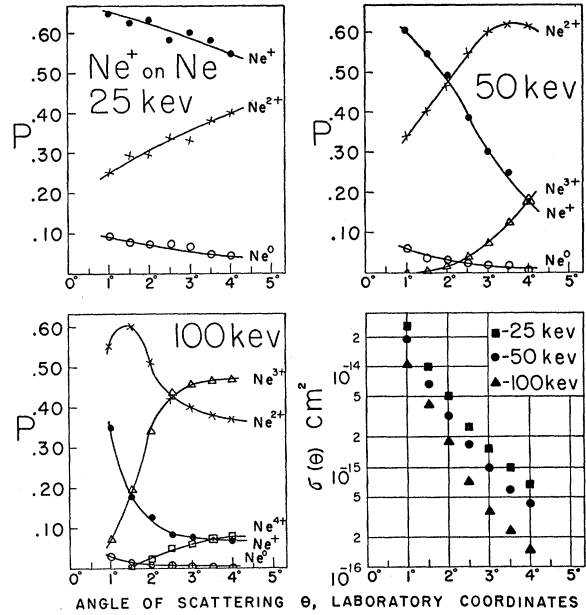


FIG. 5. The charge analysis and differential scattering cross sections for single collisions of  $\text{Ne}^+$  on Ne at 25, 50, and 100 keV. The fraction of scattered particles in each charge state is plotted *vs* scattering angle and empirical lines drawn through the data points. The differential cross section is plotted *vs* scattering angle. These data are an extension to small angles of the data in Figs. 7 and 13 of reference II.

outside the chamber accounted for the size of the effect. The presence of this effect was determined by a simple experiment. The particle current was recorded

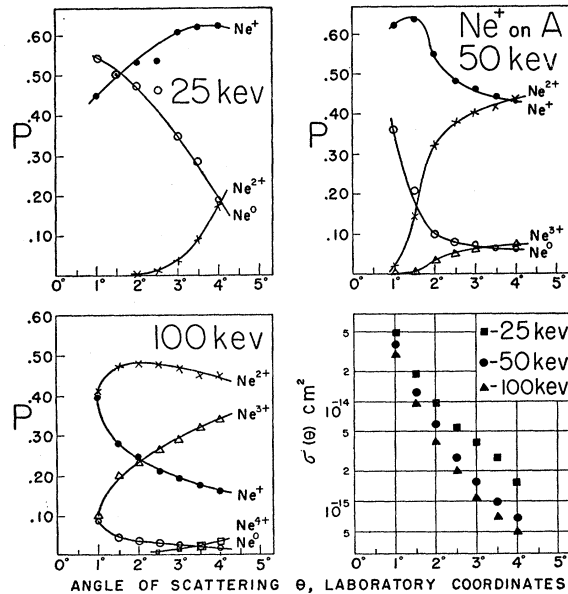


FIG. 6. The charge analysis and differential scattering cross sections for single collisions of  $\text{Ne}^+$  on A at 25, 50, and 100 keV. The fraction of scattered particles in each charge state is plotted *vs* scattering angle and empirical lines drawn through the data points. The differential cross section is plotted *vs* scattering angle. These data are an extension to small angles of the data in Figs. 8 and 14 of reference II.

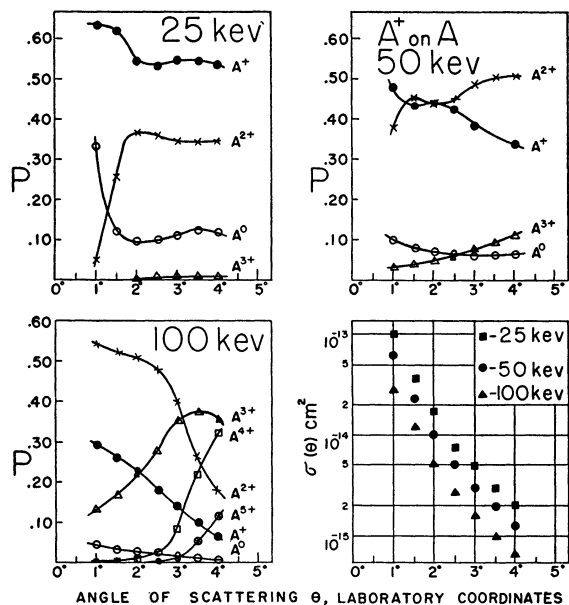


FIG. 7. The charge analysis and differential scattering cross sections for single collisions  $A^+$  on  $A$  at 25, 50, and 100 keV. The fraction of scattered particles in each charge state is plotted vs scattering angle and empirical lines drawn through the data points. The differential cross section is plotted vs scattering angle. These data are an extension to small angles of the data in Figs. 9 and 15 of reference II.

as a function of the time after the target gas supply to the collision chamber was cut off. It was observed that the current fell off very rapidly in the first 5 or 10 seconds, and then much more slowly for the next 120 seconds at which time it had essentially reached the steady value shown at zero pressure in Fig. 8. After one subtracts this steady value the current may be plotted vs time as shown in Fig. 9.

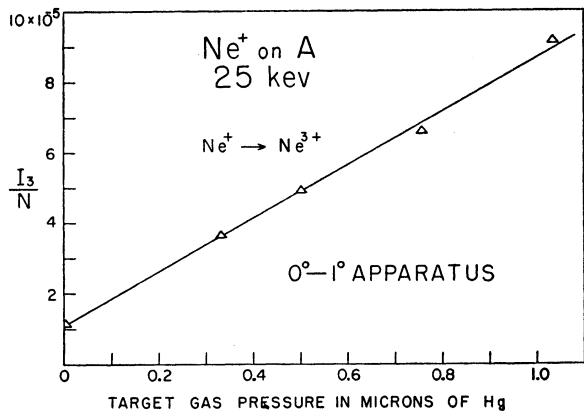


FIG. 8. The ratio of three times ionized neon particle current to incident ion particle current vs target gas pressure for single collisions of  $Ne^+$  on  $A$  at 25 keV. The linearity of the data indicates the predominance of single interactions. The ordinate intercept is the value of the residual effects and the slope of the line yields the contribution to  $\sigma_{13}$  from the 0 to 1 degree range.

The explanation of this behavior is that the collision chamber was pumped out through holes  $a$  and  $c$  to a small fraction of its original target gas pressure in just a few seconds while the much larger volume of target gas at lower pressure surrounding the chamber was reduced in pressure rather slowly once its supply from the chamber was cut off. The target gas pressures in these two regions are then exponential functions of time with rather different time constants.

In Fig. 9, where the relative current of target gas scattered particles is plotted on a logarithmic scale vs time on a linear scale, the points for time greater than 20 seconds are indeed found to fall in a straight line. It is evident upon extrapolating this line back to time zero that 23% of the current results from interactions with target gas atoms outside of the chamber and 77%

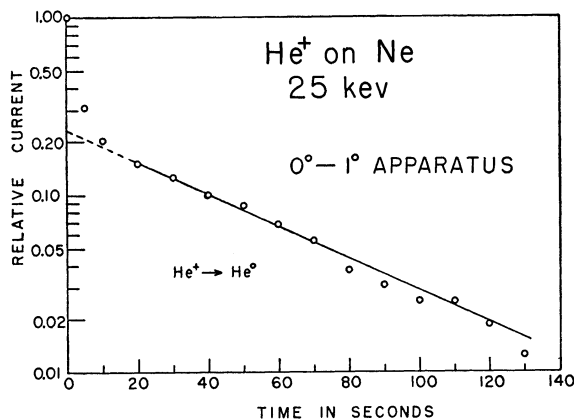


FIG. 9. The relative current of neutral helium atoms vs time for single collisions of  $He^+$  on  $Ne$  at 25 keV. The target gas supply to the collision chamber was shut off at time zero. The residual value of current reached after several minutes has been subtracted so that each point represents the current resulting from interactions with target gas atoms only. The straight line portion of the data extrapolated back to time zero yields the relative contribution from target gas atoms outside of the collision chamber.

from those inside. These percentages were found to be independent (within 2%) of the charge state detected, the kind of target gas, and the kind and energy of incident ion. This effect was taken into account by using for  $l$  in Eq. (4) an effective length equal to  $1.00/0.77$  or 1.30 times the actual length of the collision chamber.

Another correction must be applied to Eq. (4) in order that  $\sigma_{1n}^*(0^\circ \rightarrow 1^\circ)$  may represent the contribution to  $\sigma_{1n}$  from the 0 to 1 degree region only. Particles deflected through angles up to  $1\frac{1}{4}$  degrees reach the detectors when they are scattered from target atoms near  $c$ , and it is necessary to correct for those scattered more than 1 degree. The amount to be subtracted is easily computed since the scattering geometry is known and the differential cross section for each of the processes under study has been determined at 1 degree and

1½ degrees as described in Sec. 2 above. In most cases this correction was small, although in a few instances where the differential cross section for the process in question was rising sharply with increasing angle at 1 degree the correction reached 20%. In these few cases the contribution to  $\sigma_{1n}$  from the 0 to 1 degree region was small compared with that from the large-angle region.

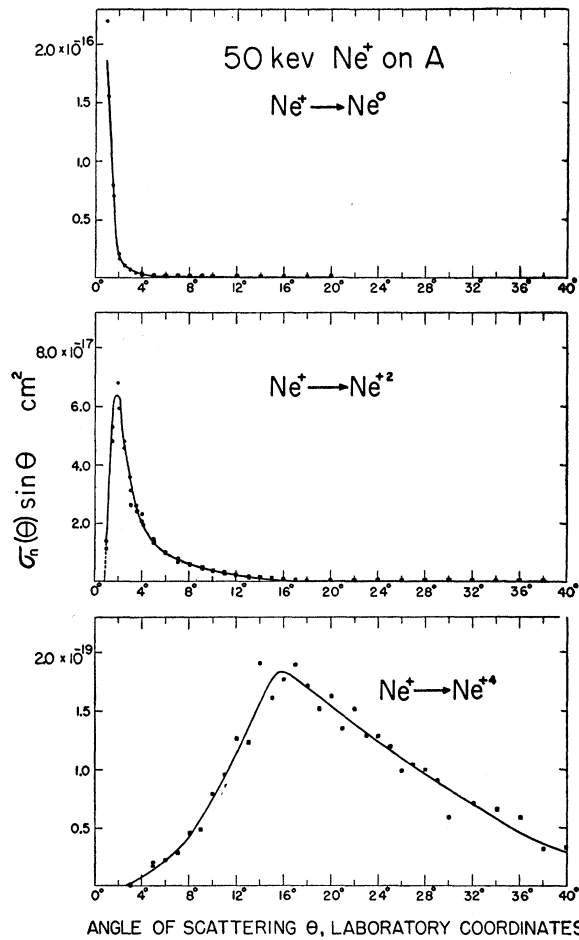


FIG. 10. The process differential cross section weighted by  $\sin\theta$  vs scattering angle for single collisions of  $\text{Ne}^+$  on A at 50 keV. The processes  $\text{Ne}^+ \rightarrow \text{Ne}^0$ ,  $\text{Ne}^+ \rightarrow \text{Ne}^{2+}$ , and  $\text{Ne}^+ \rightarrow \text{Ne}^{4+}$  are shown. Empirical lines are drawn through the data points. The area under the curve gives the contribution from the 1 to 40 degree range to the total cross section for the process in question.

c. Data and Discussion

The relative contribution from the 0 to 1 degree range is shown in column 5 of Tables I, II, and III. The absolute value of the contribution may be obtained by taking this percentage of the entry in column 4, which is the measured total cross section for the process. The discussion of these data and their relation to the contributions from the other angular regions is given in Sec. 4.

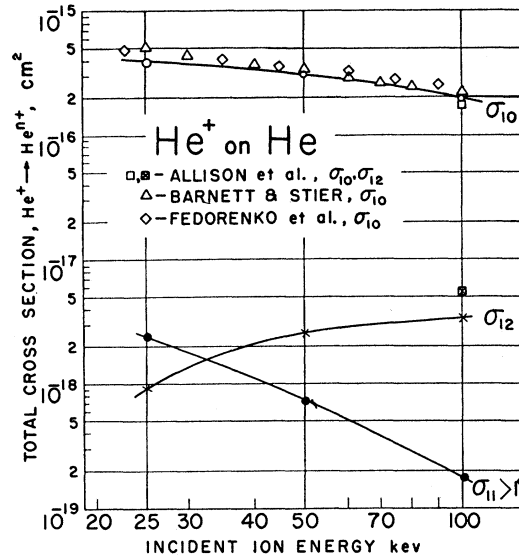


FIG. 11. The total cross sections for electron capture  $\sigma_{10}$ , elastic scattering through angles greater than 1 degree  $\sigma_{11} > 1^\circ$ , and electron loss  $\sigma_{12}$  vs incident ion energy.  $\text{He}^+$  ions are incident on neutral He gas atoms. Empirical lines are drawn through the data points of the present paper.

4. TOTAL CROSS SECTIONS

a. Method of Compiling

The total cross section  $\sigma_{1n}$  for the production of  $n$ -times ionized particles from singly ionized incident ions is the effective area of the target gas atom for the process. For a particular process the scattered incident particles in the given charge state have a certain angular

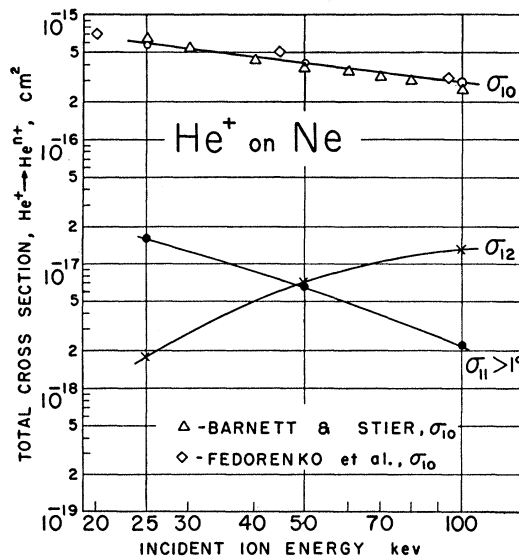


FIG. 12. The total cross sections for electron capture  $\sigma_{10}$ , elastic scattering through angles greater than 1 degree  $\sigma_{11} > 1^\circ$ , and electron loss  $\sigma_{12}$  vs incident ion energy.  $\text{He}^+$  ions are incident on neutral Ne gas atoms. Empirical lines are drawn through the data points of the present paper.

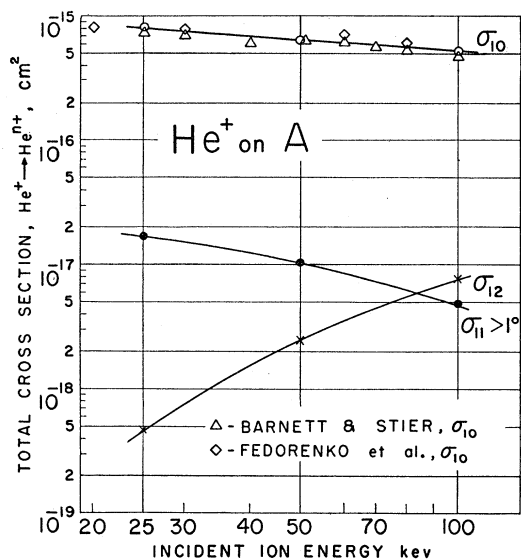


FIG. 13. The total cross sections for electron capture  $\sigma_{10}$ , elastic scattering through angles greater than 1 degree  $\sigma_{11} > 1^\circ$ , and electron loss  $\sigma_{12}$  vs incident ion energy.  $\text{He}^+$  ions are incident on neutral A gas atoms. Empirical lines are drawn through the data points of the present paper.

distribution which can be designated by the differential cross section for the process  $\sigma_n(\theta) \equiv P_n(\theta)\sigma(\theta)$ . The fraction  $P_n$  of the particles in each charge state, and the particle differential cross section  $\sigma(\theta)$  were obtained

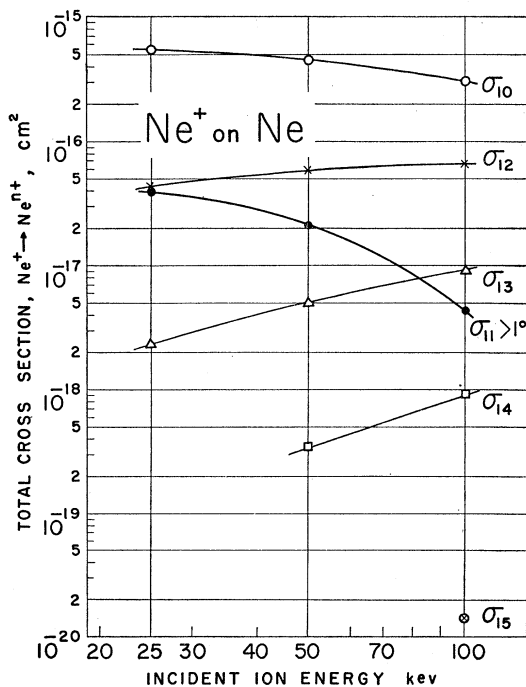


FIG. 14. The total cross sections for electron capture  $\sigma_{10}$ , elastic scattering through angles greater than 1 degree  $\sigma_{11} > 1^\circ$ , and various degrees of stripping  $\sigma_{12}, \dots, \sigma_{15}$  vs incident ion energy.  $\text{Ne}^+$  ions are incident on neutral Ne gas atoms. Empirical lines are drawn through the data points.

at each scattering angle  $\theta$ , as indicated above and in II. The contribution to  $\sigma_{1n}$  by collisions which produce  $n$ -times ionized particles at scattering angles between  $\theta_a$  and  $\theta_b$  may then be obtained by integrating the differential cross section for the process, so that

$$\sigma_{1n}^*(\theta_a \rightarrow \theta_b) = 2\pi \int_{\theta_a}^{\theta_b} \sigma_n(\theta) \sin\theta d\theta. \quad (5)$$

Thus, the contribution to  $\sigma_{1n}$  from a particular angular region may be computed from Eq. (5) anywhere within the range of the angular measurements. The integration was done numerically over the 1 to 4 degree region using the data of Sec. 2, and over the regions beyond 4 degrees using the data of II. The integrand appearing in Eq. (5) is plotted in Fig. 10 as a function of  $\theta$  for three typical cases, showing how different angular regions contribute to the total cross section. In each case the integrand is plotted up to a maximum angle  $\theta_1$  which is the largest angle for which the differential data is known.

An estimate of the contribution to  $\sigma_{1n}$  from the region between  $\theta_1$  and 180 degrees was made in the following way: It can be observed from the data of II that the fraction  $P_n$  of scattered particles in a given charge state shows little variation with angle for the higher charge states at large angles. Thus, if the impact parameter  $b$  corresponding to the angle of scattering  $\theta_1$  were known, the contribution to  $\sigma_{1n}$  from the  $\theta_1$  to 180 degree region could be obtained at once as

$$\sigma_{1n}^*(\theta_1 \rightarrow 180^\circ) = P_n(\theta_1)\pi b^2. \quad (6)$$

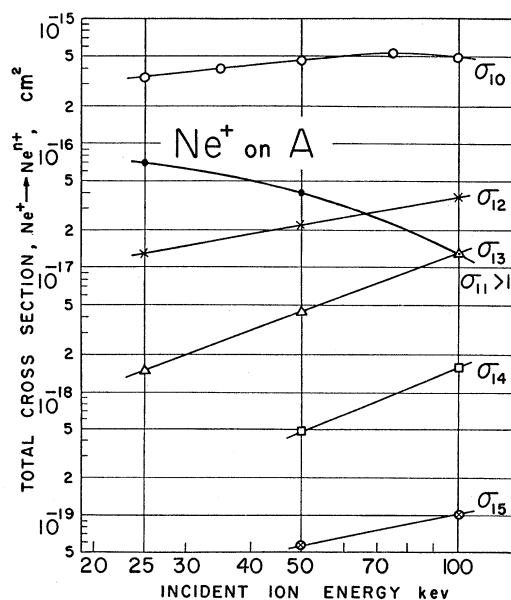


FIG. 15. The total cross sections for electron capture  $\sigma_{10}$ , elastic scattering through angles greater than 1 degree  $\sigma_{11} > 1^\circ$ , and various degrees of stripping  $\sigma_{12}, \dots, \sigma_{15}$  vs incident ion energy.  $\text{Ne}^+$  ions are incident on neutral A gas atoms. Empirical lines are drawn through the data points.

The impact parameter  $p$  was determined on the basis of a calculation by one of the present authors<sup>6</sup> in which the particle differential scattering cross section was calculated for a Coulomb potential with exponential screening. In the great majority of the cases, including all cases where  $\text{He}^+$  ions were the incident particles, this term was negligible.

The contribution to  $\sigma_{1n}$  from the 0 to 1 degree region was obtained as indicated in Sec. 3 and the total cross section  $\sigma_{1n}$  obtained as the sum of the contributions from the various angular regions:

$$\sigma_{1n} = \sigma_{1n}^*(0^\circ \rightarrow 1^\circ) + \sigma_{1n}^*(1^\circ \rightarrow 4^\circ) + \sigma_{1n}^*(4^\circ \rightarrow \theta_1) + \sigma_{1n}^*(\theta_1 \rightarrow 180^\circ). \quad (7)$$

**b. Data and Discussion**

Figures 11 through 17 show the measured values of the total cross sections  $\sigma_{1n}$  as a function of incident ion energy. The data of other authors are shown for comparison where available. Empirical lines are drawn through our data points.

The electron capture cross section  $\sigma_{10}$  for  $\text{He}^+$  ions in helium, neon, and argon gases has been reported by Barnett and Stier<sup>7</sup> and by Fedorenko, Afrosimov,

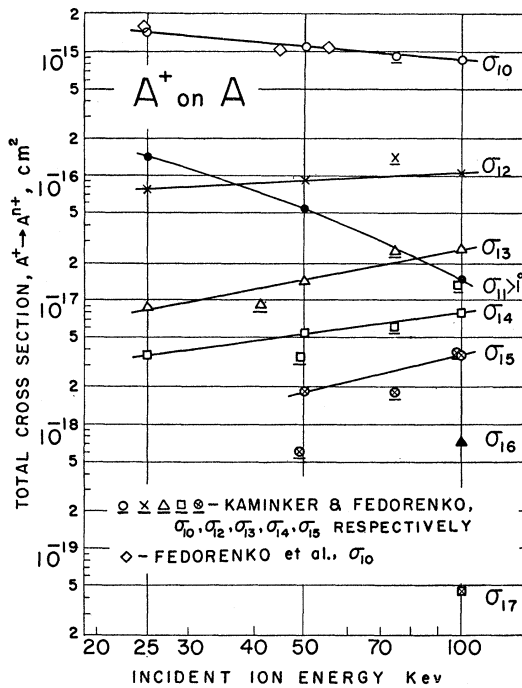


FIG. 16. The total cross sections for electron capture  $\sigma_{10}$ , elastic scattering through angles greater than 1 degree  $\sigma_{11} > 1^\circ$ , and various degrees of stripping  $\sigma_{12}, \dots, \sigma_{17}$  vs incident ion energy.  $\text{A}^+$  ions are incident on neutral A gas atoms. Empirical lines are drawn through the data points of the present paper, except those for  $\sigma_{16}$  and  $\sigma_{17}$  which were determined at only one energy.

<sup>6</sup> Everhart, Stone, and Carbone, Phys. Rev. **99**, 1287 (1955).  
<sup>7</sup> C. F. Barnett and P. M. Stier, Phys. Rev. **109**, 385 (1958).

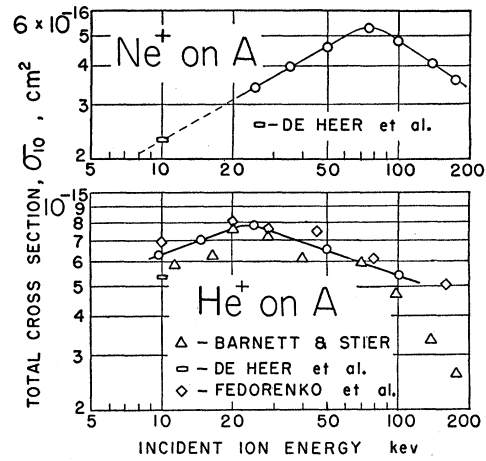


FIG. 17. The total cross section for electron capture vs incident ion energy for single collisions of  $\text{Ne}^+$  on A and  $\text{He}^+$  on A. Empirical lines are drawn through the data points of the present paper as indicated by the open circles.

and Kaminker.<sup>8</sup> In addition Allison, Cuevas, and Murphy<sup>9</sup> give measured values of  $\sigma_{10}$  and  $\sigma_{12}$  for  $\text{He}^+$  ions in helium gas. The data of these authors as well as our data are shown in Figs. 11 through 13. The agreement among these various determinations is seen to be generally good.

The remaining cases of  $\text{Ne}^+$  ions in neon and argon gases, and  $\text{A}^+$  ions in argon gas, are shown in Figs. 14 through 16. Here it was possible to compare the various cross sections for  $\text{A}^+$  ions in argon gas with those obtained by Kaminker and Fedorenko<sup>4</sup> and by Fedorenko *et al.*<sup>8</sup> Figure 16 shows that there is some difference in the slopes of the cross sections vs energy for the higher charge states as obtained by this laboratory and by Kaminker and Fedorenko. The data presented here have been obtained over a larger angular range than those of Kaminker and Fedorenko whose measurements extend to 15 degrees. Therefore it may be significant that our data points lie well above theirs in just those cases where very-large-angle scattering was found to make an important contribution. Despite these differences the agreement between our data and those of Kaminker and Fedorenko is generally good.

A maximum in the electron capture cross section  $\sigma_{10}$  as a function of incident ion energy was observed to lie within the 25 to 100 kev energy range for both  $\text{He}^+$  and  $\text{Ne}^+$  ions in argon gas. Additional measurements of  $\sigma_{10}$  were made in each of these two cases at a number of energies between 10 and 175 kev in order to more definitely establish the location of these maxima. In both cases comparison could be made with the data of DeHeer, Huizenga, and Kistemaker,<sup>10</sup> as well as with

<sup>8</sup> Fedorenko, Afrosimov, and Kaminker, Zhur. Tekh. Fiz. **26**, 1929 (1956) [translation: Soviet Phys. (Tech. Phys.) **1**, 1861 (1957)].

<sup>9</sup> Allison, Cuevas, and Murphy, Phys. Rev. **102**, 1041 (1956).

<sup>10</sup> DeHeer, Huizenga, and Kistemakeir, Physca **23**, 181 (1957).

TABLE I. The total cross section  $\sigma_{1n}$  for the process  $\text{He}^+ \rightarrow \text{He}^{n+}$  and the percent of  $\sigma_{1n}$  contributed by various angular regions are shown. Helium ions of 25-, 50-, and 100-keV energy are incident upon helium, neon, and argon gas targets.

Target gas	$n$	$E$ (keV)	$\sigma_{1n}(10^{-17}\text{cm}^2)$	% ( $0^\circ \rightarrow 1^\circ$ )	% ( $1^\circ \rightarrow 4^\circ$ )	% ( $4^\circ \rightarrow \infty$ )	$\theta_1$
He	0	25	38	99.6	0.34	0.016	12°
		50	30	99.7	0.27	0.019	14°
		100	19	99.95	0.05	0.002	14°
	1	25	0.24	...	93	7	12°
		50	0.074	...	96	4	14°
		100	0.018	...	95	5	14°
	2	25	0.093	88.1	11	0.9	12°
		50	0.26	98.9	1.0	0.07	14°
		100	0.34	99.5	0.5	0.03	14°
Ne	0	25	58	97.9	1.8	0.26	12°
		50	40	99.3	0.70	0.080	22°
		100	29	99.8	0.17	0.022	24°
	1	25	1.6	...	87	13	12°
		50	0.65	...	89	11	22°
		100	0.22	...	90	10	24°
	2	25	0.18	64	31	4.8	12°
		50	0.71	87	11	1.7	22°
		100	1.3	94	5.3	0.57	24°
A	0	25	78	96.0	3.4	0.55	20°
		50	64	98.7	1.1	0.17	20°
		100	53	99.3	0.57	0.10	20°
	1	25	1.7	...	82	18	20°
		50	1.04	...	85	15	20°
		100	0.48	...	86	14	20°
	2	25	0.047	36	49	15	20°
		50	0.25	83	14	3.0	20°
		100	0.77	97	2.5	0.6	20°

TABLE II. The total cross section  $\sigma_{1n}$  for the process  $\text{Ne}^+ \rightarrow \text{Ne}^{n+}$  and the percent of  $\sigma_{1n}$  contributed by various angular regions are shown. Neon ions of 25-, 50-, and 100-keV energy are incident upon neon and argon gas targets.

Target gas	$n$	$E$ (keV)	$\sigma_{1n}(10^{-17}\text{cm}^2)$	% ( $0^\circ \rightarrow 1^\circ$ )	% ( $1^\circ \rightarrow 4^\circ$ )	% ( $4^\circ \rightarrow \theta_1$ )	% ( $> \theta_1$ )	$\theta_1$
Ne	0	25	54	99.2	0.73	0.10	~0	28°
		50	44	99.7	0.30	0.027	~0	28°
		100	30	99.9	0.10	0.015	~0	28°
	1	25	3.9	...	84	16	~0	28°
		50	2.1	...	94	6	~0	28°
		100	0.43	...	94	6	~0	28°
	2	25	4.3	37	37.5	23.5	2.0	28°
		50	5.8	63	31.5	5.0	0.5	28°
		100	6.5	79	19	2.0	~0	28°
	3	25	0.23	1.0	...	82	17	30°
		50	0.49	3.5	23	69	4.5	28°
		100	0.93	15	61	23	1.0	28°
	4	50	0.034	<0.5	3.7	79	17	28°
		100	0.092	3.5	41	53.5	5.2	28°
	5	100	0.0014	...	...	84	16	23°
A	0	25	34	84.6	14	1.4	~0	40°
		50	46	97.3	2.4	0.25	~0	40°
		100	48	99.6	0.39	0.049	~0	40°
	1	25	7.1	...	75	25	~0	40°
		50	4.1	...	86	14	~0	40°
		100	1.3	...	90	10	~0	40°
	2	25	1.3	0.9	14.5	80	4.4	40°
		50	2.2	5.0	59	35	0.8	40°
		100	3.7	41	52	6.9	~0	40°
	3	25	0.15	<0.1	3.0	79	18	38°
		50	0.43	<0.5	30	65	5.3	40°
		100	1.3	10	66	24	~0	40°
	4	50	0.048	...	<2	79	21	40°
		100	0.16	<0.5	14	82	3.8	40°
	5	50	0.0056	...	...	57	43	40°
		100	0.010	...	<1.0	89	11	38°

TABLE III. The total cross section  $\sigma_{1n}$  for the process  $A^+ \rightarrow A^{n+}$  and the percent of  $\sigma_{1n}$  contributed by various angular regions are shown. Argon ions of 25-, 50-, and 100-keV energy are incident upon an argon gas target.

Target gas	$n$	$E$ (keV)	$\sigma_{1n}(10^{-17}\text{cm}^2)$	% ( $0^\circ \rightarrow 1^\circ$ )	% ( $1^\circ \rightarrow 4^\circ$ )	% ( $4^\circ \rightarrow \theta_1$ )	% ( $> \theta_1$ )	$\theta_1$
A	0	25	140	97.4	2.2	0.37	~0	$32^\circ$
		50	110	99.1	0.80	0.10	~0	$36^\circ$
		100	85	99.8	0.23	0.011	~0	$36^\circ$
	1	25	14	...	84	16	~0	$32^\circ$
		50	5.4	...	91	9.0	~0	$36^\circ$
		100	1.4	...	97	3.0	~0	$36^\circ$
	2	25	7.8	4.9	67	27	1.2	$32^\circ$
		50	9.2	34	54	12	0.15	$36^\circ$
		100	10.5	70	29	1.3	~0	$36^\circ$
	3	25	.88	0.10	17	61	22	$32^\circ$
		50	1.4	11	32	54	2.8	$36^\circ$
		100	2.6	31	52	17	~0	$36^\circ$
	4	25	0.36	...	...	59	41	$32^\circ$
		50	0.53	<0.40	0.35	90	9.7	$36^\circ$
		100	0.78	<2.0	30	69	1.0	$36^\circ$
	5	50	0.18	<0.10	<0.10	85	15	$36^\circ$
		100	0.36	<0.10	11	85	4	$36^\circ$
		100	0.073	<0.50	26	60	14	$36^\circ$
	7	100	0.0044	...	...	45	55	$36^\circ$

the data of the previously mentioned authors in the case of  $\text{He}^+$  in argon gas. Figure 17 shows these data in the extended energy range.

It can be observed quite generally from the figures that in the energy range of this investigation the electron capture process is by far the most probable one and that the electron stripping processes occur with decreasing probability for increasing numbers of electrons removed. Except for the two cases noted,  $\sigma_{10}$  is seen to be a decreasing function of incident ion energy, while the stripping cross sections are all observed to be increasing functions of energy.

Tables I, II, and III show the relative contribution to each of the cross sections  $\sigma_{1n}$  by the various angular regions. Since the cross section  $\sigma_{11}$  is for "elastic" scattering through angles greater than 1 degree there is no 0 to 1 degree contribution listed for it. For all of

the other cross sections the relative contribution of the 0 to 1 degree region is seen to increase with increasing incident ion energy. Also, for the collision of a specific ion and target atom at a particular energy, the relative contribution from the 0 to 1 degree region always decreases with increasing degree of ionization (increasing  $n$ ). Thus large-angle scattering generally becomes more important with both decreasing incident ion energy and increasing charge state of the scattered particle. A comparison of Tables I, II, and III, in which  $\text{He}^+$ ,  $\text{Ne}^+$ , and  $\text{A}^+$ , respectively, are the incident particles, shows also that large-angle scattering is more important for collisions of the heavier atoms.

In conclusion we should like to express our appreciation to Dr. Arnold Russek for discussions of the experiment and suggestions in the preparation of this paper.